



# Probing beneath the surface without a scratch – Bulk non-destructive elemental analysis using negative muons<sup>☆</sup>



A.D. Hillier<sup>a,\*</sup>, D.McK. Paul<sup>b</sup>, K. Ishida<sup>c</sup>

<sup>a</sup> ISIS facility, Rutherford Appleton Laboratory, Harwell Oxford, Didcot OX11 0QX, United Kingdom

<sup>b</sup> Department of Physics, University of Warwick, Coventry CV4 7AL, United Kingdom

<sup>c</sup> RIKEN Nishina Center, RIKEN, Wako, Saitama, Japan

## ARTICLE INFO

### Article history:

Received 4 August 2015

Received in revised form 17 November 2015

Accepted 17 November 2015

Available online 22 November 2015

### Keywords:

Elemental analysis

Negative muons

Non-destructive

Depth profiling

## ABSTRACT

The development of elemental analysis at the ISIS pulsed neutron and muon facility, STFC Rutherford Appleton Laboratory, UK, is described. Presented are recent results from the calibration of the new setup and this shows the technique can be a powerful tool in determining the composition of materials in bulk, not just at the surface. Moreover, this technique is non-destructive and should be sensitive to all elements (perhaps with the exception of H and He).

© 2015 Elsevier B.V. All rights reserved.

## 1. Introduction

Elemental analysis is a process in which a sample is analyzed for its composition. Often this is accomplished by destructive and damaging methods. Clearly, such techniques are not desirable for valuable items; cultural scientific or monetary, and a non-destructive, non-damaging elemental analysis would be extremely useful. Such a tool can be found in the use of negative muons, where the absorption process releases characteristic X-rays from the elements present.

Negative muons are comparable to heavy electrons; replacing an electron in the outer shell of an atom, then traveling to near the nucleus through the modified energy states of the atom. Each transition on this path produces an X-ray characteristic of the atom in which the muon was absorbed, hence allowing this spectrum to reflect the atomic species (see Fig. 1). The sensitivity of this technique is such that even light atoms can be detected. Furthermore the technique has the potential to be used as a depth analysis tool, since by varying the depth of implantation of the negative muon. A significant advantage of muonic X-rays over those of electronic X-rays is their higher energy (2 keV–10 MeV) (see Fig. 2). These high energy muonic X-rays are emitted from the bulk of the samples without the added complication of photon self-

absorption and can be simply detected by a semiconductor detector. From Fig. 2 we can see that the X-ray emission energy scales with  $Z$  (see ref [1] for a more detailed review). In addition, this technique will not activate the sample, unlike prompt gamma-ray analysis by neutron irradiation. Over the years there has been sporadic use of negative muons as an elemental analysis tool, and a wide-ranging number of materials have been investigated, including Japanese coins [1], spinal columns [2], pig fat and dog's blood [3], tissue analysis [4], ancient Chinese mirrors and Tang San Cai horse [5] and even meteorite composition [6]. Recently, an instrument has been constructed at the J-PARC facility [7]. ISIS pulsed neutron and muon facility is a primary high-flux source of pulsed muon beams. In this paper we will discuss the latest developments at ISIS and the possible uses for the future.

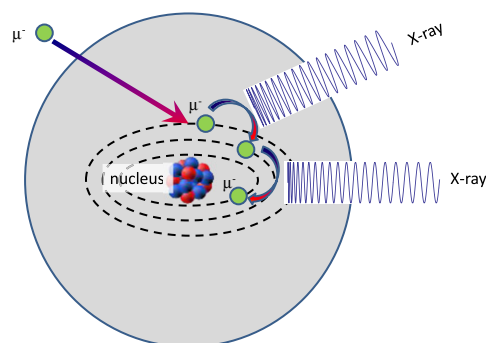


Fig. 1. A schematic diagram which shows the  $\mu$ -capture and X-ray emission process.

<sup>☆</sup> Selected papers presented at TECHNART 2015 Conference, Catania (Italy), April 27–30, 2015.

\* Corresponding author at: Rutherford Appleton Laboratory, ISIS, Harwell Oxford, Didcot OX11 0QX, United Kingdom.

E-mail address: [adrian.hillier@stfc.ac.uk](mailto:adrian.hillier@stfc.ac.uk) (A.D. Hillier).

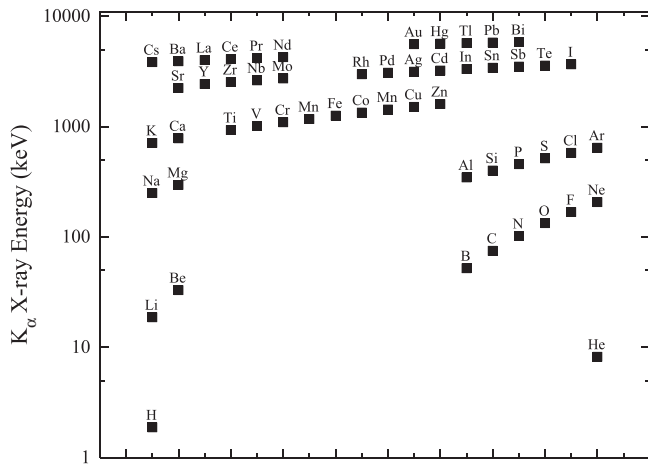


Fig. 2. The  $K_{\alpha}$  X-ray energy for various elements. The data was taken from ref. [10].

## 2. Experimental details

### 2.1. Production of a negative muon beamline at ISIS

The negative muon experiments were conducted at the ISIS pulsed neutron and muon source at the STFC Rutherford Appleton Laboratory, UK. ISIS is a proton accelerator in which protons are accelerated up to 800 MeV before colliding with a target, of which there are two: namely TS1 and TS2. The muon production target is on the first target station and is located 30 m in front of the neutron target. The muon target is 10 mm thick (along the beam axis) and is made of carbon. The interaction of protons and the carbon nuclei produces pions and these pions decay into muons. The special nature of the RIKEN beamlines allows both positive and negative muons to be transported to the experimental area, in this case port 4 the home of CHRONUS, (see Fig. 3). For information on the RIKEN beamlines see ref. [9] and for the CHRONUS spectrometer see ref. [10]. In addition, the beamline can be tuned for a range of momenta, in this case from 20 MeV/c to 90 MeV/c. This allows for a

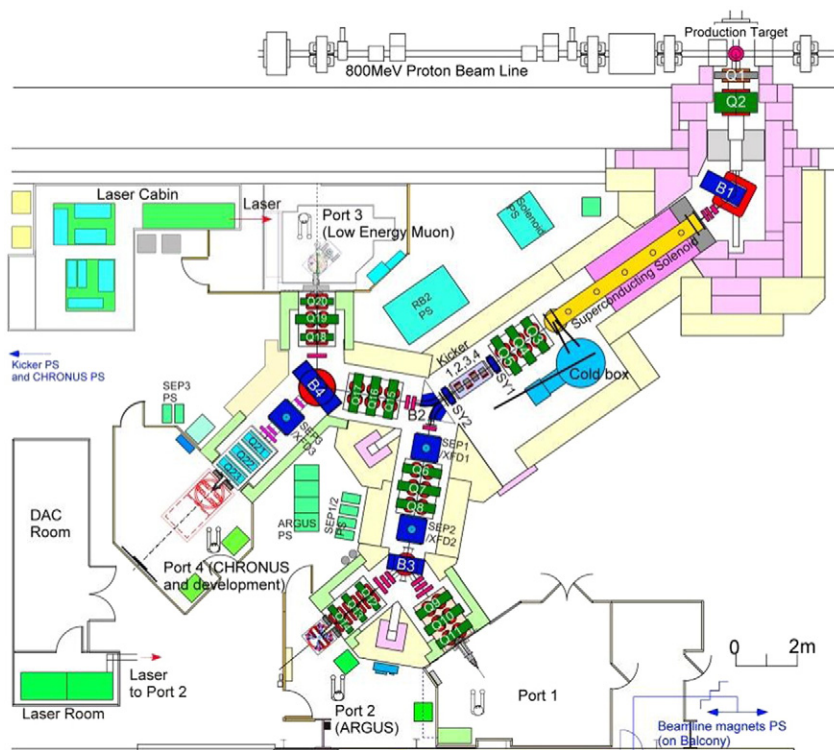


Fig. 3. A schematic layout of the RIKEN-RAL beamlines, port 4 (the home of CHRONUS) is the experimental area used in these measurements.

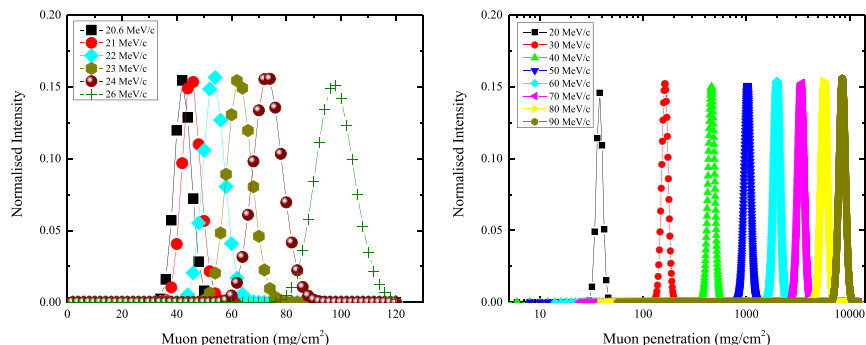
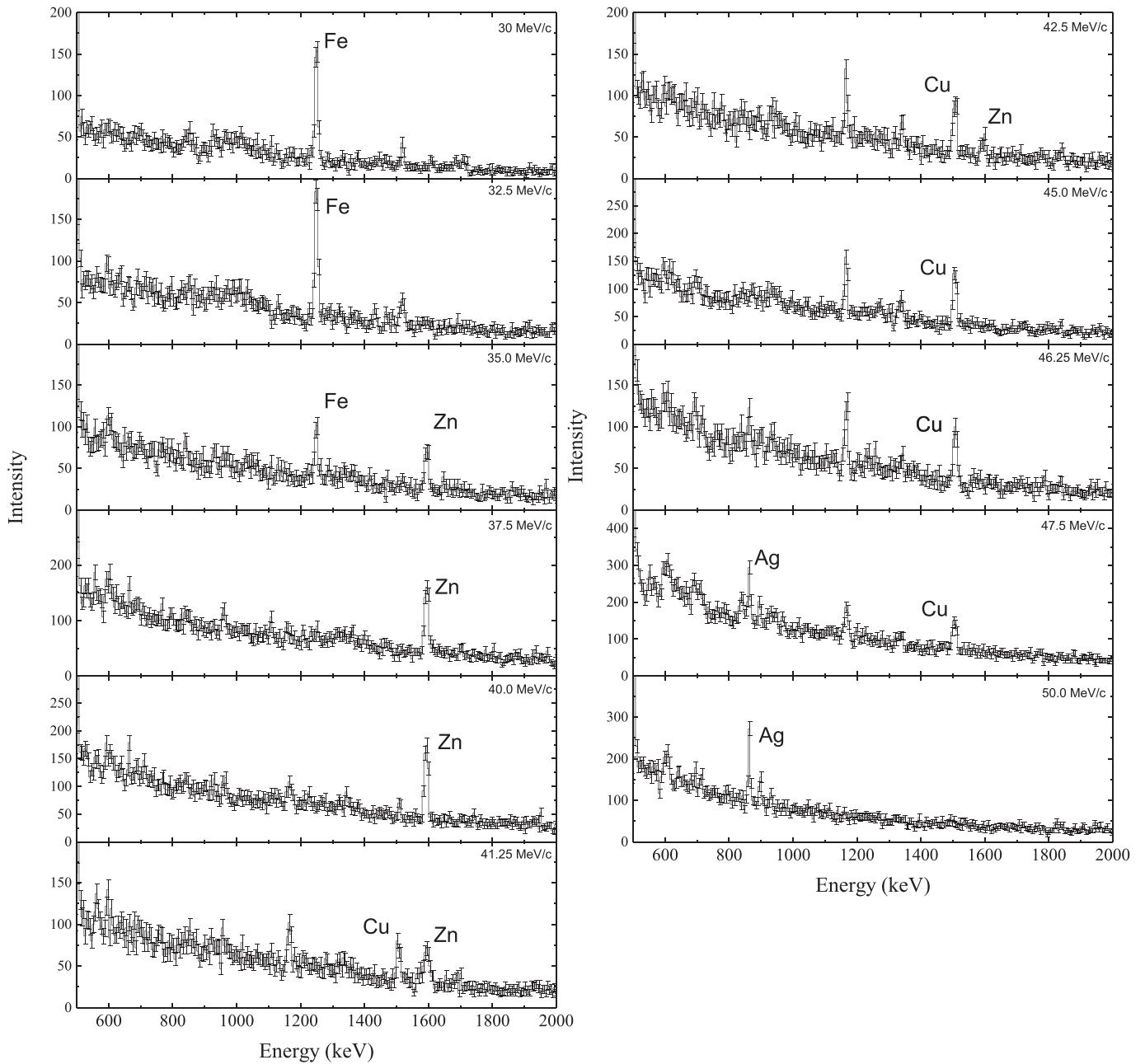


Fig. 4. A simulation of the implantation depth of the muons as a function of incident momenta.



**Fig. 5.** Photographs of the experiment setup. The picture on the left is the view from above and the picture on the right is from the side. The aerial picture shows the layout and angles of the detectors to the sample. The side view shows a sample being held in place.



**Fig. 6.** This figure shows the momentum dependence of the X-ray emission. The lowest momentum shows just the Fe X-ray peaks and the highest shows just the Ag X-ray peaks, with Zn and Cu at intermediate muon momentum. This data is from one detector only.

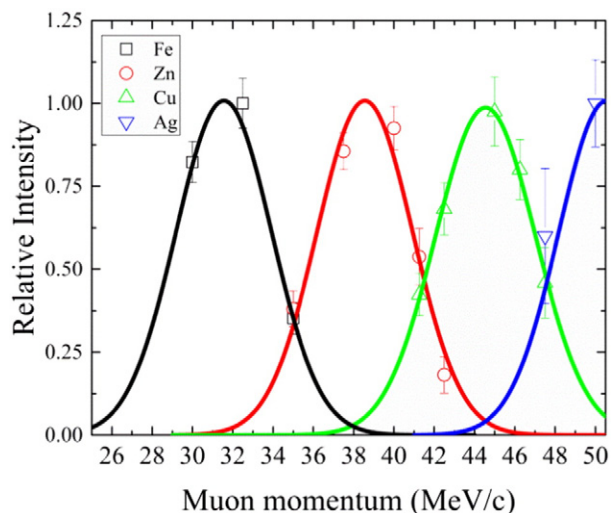


Fig. 7. The integrated intensity of the element X-ray emission peaks as a function of muon momentum.

controlled implantation depth (see Fig. 4). As can be seen, the implantation depth can be varied from  $0.4/\rho$  mm to nearly  $100/\rho$  mm, obviously this is density dependent,  $\rho$  in  $\text{g}/\text{cm}^3$ . For example, in water the implantation depth range is from 0.4 to 100 mm and for Cu is from 0.05 to 11.2 mm. Of course, as the implantation depth is increased then the momenta spread increases due to the scattering of the muons and the fixed fractional momentum bite. This controllability of the muon momentum allows for elemental analysis as a function of depth to be measured. Indeed, this allows for elemental analysis below the surface (which could be corroded and/or have been tampered with).

Table 1

The certified composition for the two bronze standards. The ratio of the peak intensities from the muonic X-rays. This shows a remarkably good agreement. The abbreviations n.d. indicates not detected and n.c. not calculated. This is due to the potential contamination of the data due to the lead beam snout.

Element	Standard A		Standard C	
	Certified composition (%)	Ratio of peak intensity to Cu (%)	Certified composition (%)	Ratio of peak intensity to Cu (%)
As	$0.194 \pm 0.1$	$0.5 \pm 0.3$	$4.60 \pm 0.27$	$4.4 \pm 0.5$
Pb	$7.9 \pm 0.7$	n.c.	$0.175 \pm 0.014$	n.c.
Sn	$7.16 \pm 0.21$	$7.5 \pm 0.5$	$0.202 \pm 0.029$	$0.6 \pm 0.3$
Zn	$6.02 \pm 0.22$	$6.1 \pm 0.5$	$0.055 \pm 0.005$	n.d.

## 2.2. Current instrument setup

The current instrument setup is shown in Fig. 5. Currently, we have installed three Ge based ORTEC X-ray detectors, along with the two electron counters. These are all placed on a flat surface. Two of the Ge detectors have an energy range from 0.1 to 10 MeV and the other has a lower energy 3 keV to 10 MeV. This lower energy detector is better suited for lighter elements, e.g. biomaterials. After some test runs it became clear that additional shielding was required to reduce the background Pb signal as the negative muon background from collisions with the final collimator was giving such a high signal. The sample itself can be held in a simple Al packet, as the muons have a high enough momentum to pass straight through.

## 3. Results and discussion

The first experiment conducted was depth profiling of a known sample. A sample of metal foils was constructed; it consisted of Fe (500  $\mu\text{m}$ ), Zn (500  $\mu\text{m}$ ), Cu (500  $\mu\text{m}$ ) and finally Ag (1000  $\mu\text{m}$ ). The muon

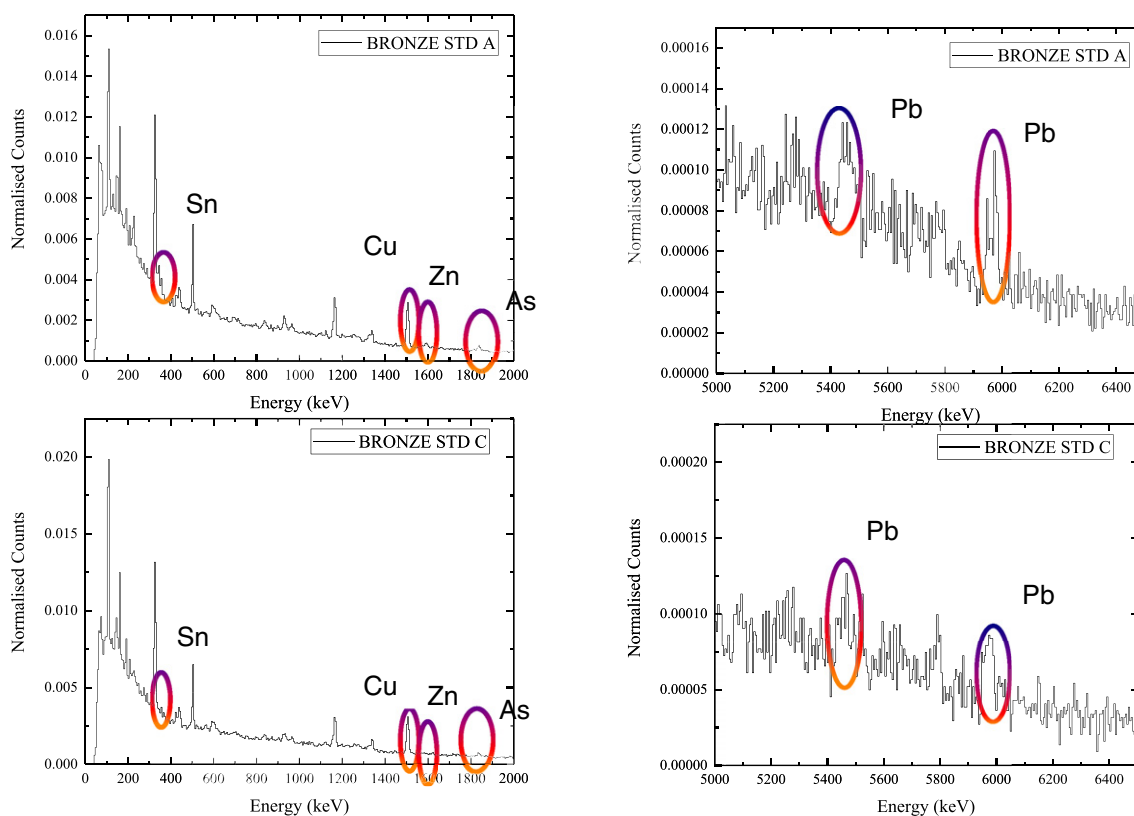


Fig. 8. The X-ray emission from the Bronze standards, clearly showing the constituent elements, Cu, Sn, Zn, As and Pb. This data is from a single detector only.

momenta were varied from 30 MeV/c to 50 MeV/c. The momenta can be varied with an accuracy of  $\pm 0.5$  MeV/c. Fig. 6 shows the X-ray emission for the different momenta. At the lowest momenta (30 MeV/c) only Fe X-ray emission was observed. As the muon momentum is increased, the Fe peak disappears and the Zn peak appears. Increasing the muon momentum still further the Zn peaks disappear and the Cu peaks appear and further still the Cu peaks disappear and only the Ag peaks remain. These results clearly show the technique as a powerful tool for depth and bulk elemental analysis, as at the highest momentum the muons passed through the first three layers without giving a signal from them and only the Ag is observed. Each spectrum was collected for less than 1 h. It is worth noting that the energies of these X-rays are of the order 1 MeV and although Fe, Zn and Cu have similar Z values they are clearly distinguishable.

Now looking at the data in more detail, the integrated intensity of each peak can be plotted as a function of muon momentum (see Fig. 7). This graph clearly shows the increase and decrease of the intensity in each peak. The line for each element is a fit to a Gaussian profile, more as a guide to the eye.

In addition to measuring the layered sample, gold and bronze standards have also been measured. The data from two bronze standards are shown in Fig. 8, with different compositions of these standards. Fig. 8 clearly demonstrates that these components can be measured. Obviously, the clearest signal is Cu but the trace elements are also observed and highlighted. By measuring the ratio of the peak intensity the composition can be determined, the results are summarised in Table 1. The Pb signal has not been calculated as there is the potential for contamination due to the beam snout. As for the other constituent elements a remarkably good agreement has been obtained.

#### 4. Conclusions

In this paper, we have shown that using negative muons as a tool for elemental analysis is possible at the ISIS pulsed neutron and muon

facility. Indeed, element analysis on a layered sample has shown controlled depth dependence studies are possible and that measurements deep within the sample are feasible. Moreover, this technique is sensitive to all elements and, of course, completely non-destructive. The bronze standards have shown the sensitivity of the technique, while only using one detector. This technique clearly has the potential to be used successfully in a wide range of applications, including engineering samples, archeological artifacts, bio-systems and battery materials. A series of experiments has commenced on Roman coins, with ones on bio-materials in the pipeline. It is hoped that by incorporating rotation and tilt measurements for a sample should be able to produce a three dimensional map of the elemental composition of a sample.

#### Acknowledgments

The authors would like to thank RIKEN-RAL for access to the beam port and STFC for the beam time and funding.

#### References

- [1] K. Ninomiya, et al., *J. Phys. Conf. Ser.* 225 (2010), 012040.
- [2] Y. Hosoi, et al., *Br. J. Radiol.* 68 (1995) 1325.
- [3] R. Hutson, et al., *Radiology* 120 (1976) 193.
- [4] J. Reidy, et al., *Analytical Chemistry* 50 (40) (1978).
- [5] M.K. Kubo, et al., *J. Radioanal. Nucl. Chem.* 278 (2008) 777.
- [6] K. Terada, et al., *Sci. Rep.* 4 (2014) 5072.
- [7] Y. Miyake, et al., *Nucl. Inst. Methods Phys. Res. A* 600 (2009) 22.
- [8] T. Mazsuzaki, et al., *Nucl. Inst. Methods Phys. Res. A* 465 (2001) 365.
- [9] D. Tomono, et al., *J. Phys. Conf. Ser.* 225 (2010) 1–4, 012056.
- [10] R. Engfer, et al., *At. Data Nucl. Data Tables* 14 (1974) 509–597.